Journal of The Electrochemical Society, **154** (12) B1315-B1324 (2007)
0013-4651/2007/154(12)/B1315/10/$20.00 © The Electrochemical Society

Validated Leverett Approach for Multiphase Flow in PEFC Diffusion Media

III. Temperature Effect and Unified Approach

E. C. Kumbur,* K. V. Sharp, and M. M. Mench,z**

Fuel Cell Dynamics and Diagnostics Laboratory, Department of Mechanical and Nuclear Engineering, The Pennsylvania State University, University Park, Pennsylvania 16802, USA

The final paper in this series is devoted to delineating the effects of temperature on the multiphase transport characteristics of thin-film polymer electrolyte fuel cell (PEFC) diffusion media (DM). Direct measurements of capillary pressure-saturation of various commercial DM coated with a wide range of poly(tetrafluoroethylene) (PTFE) loadings (from 5 to 20 wt % PTFE) were performed at different operating temperatures (20, 50, and 80°C). The benchmark data gathered from these experiments (available upon request) were compiled into the existing database generated from the first and second phase of this study, which examined the hydrophobicity and compression effects. The expanded database was then utilized to deduce a unified form of an empirical correlation appropriate for the tested DM. This semiempirical approach can predict capillary pressure of the tested DM as a function of liquid saturation, hydrophobic additive content, uncompressed porosity, compression pressure, and operating temperature within an uncertainty of ±14% of the measured capillary pressure over the entire saturation domain, showing considerable improvement over the traditional Leverett approach.
 [DOI: 10.1149/1.2784286]

Manuscript submitted March 28, 2007; revised manuscript received August 10, 2007. Available electronically October 16, 2007.

The porous fuel cell diffusion media (DM) represents a key component governing the water transport mechanism within polymer electrolyte-based fuel cells (PEFCs). It is constructed from electronically conductive carbon fiber products in the form of paper or cloth. For effective water removal purposes, the naturally hydrophilic carbon substrate is commonly impregnated with a nonuniform coating of hydrophobic agent [poly(tetrafluoroethylene) (PTFE) or other],[1,2] yielding a complex bimodal pore size distribution with mixed wettability. Because of the structurally complex internal architecture of these porous materials, it is challenging to precisely define the relatively significance of the factors controlling the governing transport parameters.

Proper tailoring of the multiphase transport in porous fuel cell DM with mixed wettability is essential for establishing the optimal microfluidic management strategy required to achieve the desired operational stability, durability, and rapid start-up from a frozen condition in PEFCs. In the open literature, the water transport phenomena are generally coupled with the fuel cell performance;[3-7] however, the specific transport characteristics of these thin-film media over a wide range of operating conditions have not been described in adequate detail. Even most efforts to model the multiphase flow in porous fuel cell media are based on bulk empirical correlations alone, and often as simplification, the wettability characteristic of the fuel cell porous media is improperly assumed to be uniform wettability.[1] To date, most fuel cell models employ a generic Leverett approach (by Leverett[8] and Udell[9]) adapted from soil science to describe the capillary-induced liquid flow through the porous fuel cell DM. This traditional approach was derived based on the experimental data of homogenous soil beds with uniform wettability[8] and therefore is incapable of capturing the mixed wettability characteristics of the fuel cell DM,[1] except through empirical fit parameters to account for the relevant effects. Even though the traditional Leverett approach is, indeed, viewed as an indispensable tool for many modelers, serving as a useful starting point toward achieving an accurate two-phase transport model in fuel cell modeling studies, the use of the traditional Leverett relationship without true validation limits the effectiveness of fuel cell models and hinders provision of reliable guidance for the design of next-generation fuel cell materials.[1]

Establishing effective microfluidic management requires a realistic description of the multiphase transport characteristics of the fuel cell DM under different operating conditions. This involves a number of material-dependent parameters, including capillary pressure, phase saturation, wettability characteristics, and different fuel cell operational environments. For instance, the DM placed in a fuel cell stack assembly is exposed to nonuniform compression, which in turn can generate strong local stresses that can alter the morphological structure and consequently, the multiphase transport characteristics of the DM.[10] Furthermore, our previous studies[11,12] revealed that along with the pore characteristics, the nonuniform distribution of the wettability can affect the capillary transport characteristics, potentially yielding discrete transport patterns. Therefore, the capillary transport characteristics of the DM tailored with different PTFE loadings at various operational environments should be precisely quantified to achieve an accurate two-phase transport model in fuel cell modeling studies.

The first and second parts of this paper series are devoted to delineating the effects of mixed wettability and assembly compression pressure on the capillary transport characteristics of a fuel cell DM. One important effect that still must be better understood is that of temperature. As repeatedly expressed in the literature,[13-16] thermal management is closely coupled with delicate water balance, which is essential to high performance and longevity of PEFCs. In terms of transport, the fuel cell DM is often exposed to a nonisothermal environment, causing significant changes in the heat and mass transport process.[15,16] Such a variation in temperature influences the governing transport properties, including permeability, the capillary pressure-saturation relation, fluid viscosity, and the surface energy of the medium, thereby directly affecting the capillary transport characteristics in fuel cell or other porous media.[17-21] Moreover, existing efforts in soil science[22-28] have revealed that the variation in equilibrium temperature is the dominating factor determining the equilibrium capillary pressure. Thus, understanding the effects of operating temperature on the capillary transport characteristics of a fuel cell DM along with knowledge of the effects of wettability characteristics and compression is of paramount importance for achieving an effective water balance and thermal management strategy in PEFCs.

This work is specifically aimed at delineating the effects of temperature on the multiphase transport characteristics of the thin-film fuel cell DM. We introduce a unified Leverett approach appropriate for tested fuel cell DM tailored with various degrees of PTFE loadings (from 5 to 20 wt %) within the range of testing conditions

* Electrochemical Society Student Member.
** Electrochemical Society Active Member.
z E-mail: mmm124@psu.edu

Table I. Material properties of the tested DM samples.[a]

Material	Type	Thickness (μm)	PTFE macro-substrates (wt %)	Porosity	Permeability (cm^3/cm^2 s)
SGL 24BC	Paper w/MPL	235	5	0.76	0.60
SGL 24CC	Paper w/MPL	235	10	0.75	0.60
SGL 24DC	Paper w/MPL	235	20	0.75	0.45
SGL 10BB	Paper w/MPL	420	5	0.84	3.00

[a] All values are adapted from manufacturer technical specification sheets. Note that the values of porosity, permeability, and PTFE content given above represent the material properties of the tested macro fuel cell diffusion media substrate (i.e., macro DM without MPL).

(temperature from 20 to 80°C and compression from 0 to 1.4 MPa). The presented approach is deduced from a wide range of capillary pressure-saturation measurements of the commercially available DM (SGL 24 series). The present empirical approach successfully predicts the measured capillary pressure-saturation behavior of the tested DM samples to within an uncertainty of ±14% of the measured values. The key feature of the unified approach is that it embodies (*i*) the nonuniform wettability characteristics of the tested DM samples, thereby accounting for the variations in transport parameters with full spatial anisotropy of the DM; and (*ii*) it accounts for the effect of compression and operating temperature on the capillary transport characteristics of the tested DM samples.

Method of Approach

SGL 24 series (SIGRACET gas diffusion layers) carbon paper DM with varying degrees of mixed wettability and SGL 10 series (SGL 10BB) carbon paper were utilized in the experiments. The same type of commercial DMs have been selected in this study to eliminate any possible uncertainties associated with the fabrication processes of these materials. These naturally hydrophilic DM are typically tailored by addition of hydrophobic material PTFE, known as Teflon, and the base macroporous substrate is coated with a microporous layer (MPL) for improved water transport. The material properties of tested DM samples supplied by the manufacturer are provided in Table I. The degree of wettability of these selected DM samples varies from 5 to 20 wt % PTFE, which is in a typical range utilized in fuel cell applications.

The method of standard porosimetry (MSP) technique developed by Porotech, Inc., was employed to measure the desired transport parameters such as capillary pressure, saturation, and hydrophobic and hydrophilic porosity distribution. The operating principle of MSP technique is explained in detail in Ref. 29, and our experimental protocol is provided in Ref. 11 and 12. The present experiments were performed at different temperatures, i.e., 20, 50, and 80°C. The DM samples were placed in contact between two standard specimens with known capillary transport characteristics for a time sufficient to achieve capillary and thermal equilibrium. At each equilibrium, the corresponding capillary pressure and saturation values were measured. Different liquids (deionized water and octane) were utilized as working fluids to evaluate the mixed wettability characteristics of DM samples over a set of different temperatures.

Results and Discussion

Effect of temperature on mixed wettability characteristics.— The bimodal pore distribution (hydrophilic and hydrophobic) and the wettability characteristics of the interfacial surface area are strongly correlated with temperature. The activity of the PTFE agent bonded on the solid carbon fibers determines the degree of wettability,

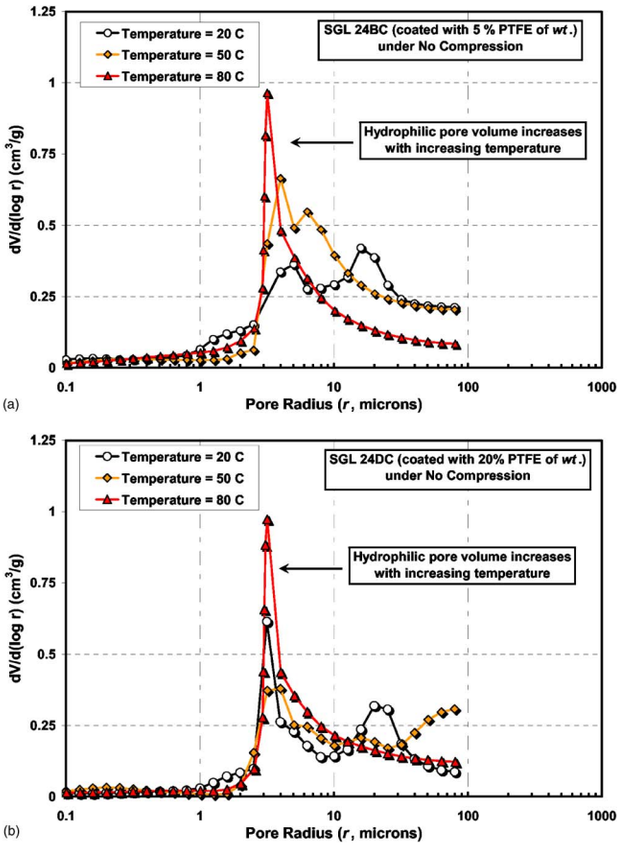

Figure 1. (Color online) Hydrophilic pore distribution at 20, 50, and 80°C of (a) SGL 24BC (5% PTFE) and (b) SGL 24DC (20% PTFE) carbon paper.

which strongly depends on the fiber temperature.[24,25] Therefore, probing the wettability characteristics of the thin-film DM at different temperatures is of utmost importance.

The hydrophilic/hydrophobic pore distribution (dual pore network) was measured by means of the MSP technique at 20, 50, and 80°C. Figure 1 shows the hydrophilic pore distribution of SGL 24BC (5% PTFE) and SGL 24DC (20% PTFE) at different temperatures. The total (hydrophilic/hydrophobic) porosity and the measured hydrophilic pore volume of the tested DM samples at different temperatures are also provided in Tables I and II, respectively. For a given DM, the hydrophilic pore distribution appears to follow a similar qualitative trend at each temperature.

To investigate the degree of change in hydrophilic pore distribution, a further comparison was performed for the tested DM samples. Figure 2 shows the hydrophilic pore distribution for SGL 24 series carbon papers at 20 and 80°C. At room temperature, a

Table II. Measured hydrophilic pore volume and hydrophilic surface area of the tested DM samples by MSP technique at different temperatures.

	Hydrophilic pore volume (cm^3)			Hydrophilic surface area (m^2/g)		
Material	20°C	50°C	80°C	20°C	50°C	80°C
SGL 24BC (5% PTFE)	0.040	0.033	0.032	54.1	49.7	58.0
SGL 24CC (10% PTFE)	0.026	0.032	0.029	41.5	41.3	59.6
SGL 24DC (20% PTFE)	0.028	0.030	0.032	49.7	41.0	55.0

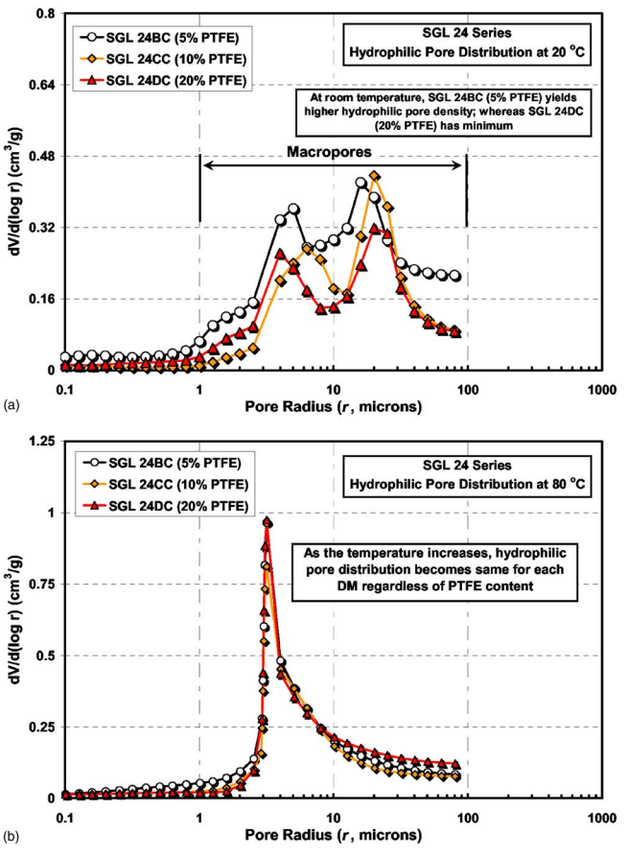

Figure 2. (Color online) Hydrophilic pore distribution of SGL 24BC (5% PTFE), SGL 24CC (10% PTFE), and SGL 24DC (20% PTFE), (a) at 20°C and (b) at 80°C.

significant deviation between the hydrophilic pore distributions of the DM samples is observed. This can be attributed to the different levels of hydrophobic agent loadings in the tested DM samples. However, as the temperature is further increased to 80°C, the hydrophilic pore distributions of the tested DM samples appear to overlap, following a similar quantitative trend regardless of PTFE loading. This observation reveals that increasing temperature contributes to a suppression of the PTFE effect through the reduction of the surface tension, leading to an increase in wettability (hydrophilic) characteristics of the pore network.

The apparent increase in hydrophilic pore volume with increasing temperature can be linked to the change in surface interaction of the fluid and solid pore matrix of the DM. Physically, the interfacial tension,[30] which is a strong function of temperature, induces wettability and capillarity, causing the fluid phases to be attracted or repelled by the solid matrix surface of the pores. Adhesion energy is defined as the molecular attraction exerted between two unlike materials in contact.[30] The hydrophobic agent PTFE bonded to the fiber matrix promotes the imbalance of the molecular forces at the interface and determines the magnitude of the instability, which is, in fact, a measure of the surface tension.[30] The surface tension and adhesion energy between the solid fiber and water are strongly linked to the activity of the PTFE particles coated on the carbon fiber.[19,22,24] Any increase in temperature is followed by the reduction of the molecular imbalance (PTFE activity) at the interface that gives rises to the adhesion energy between the water molecules and the fiber surface. The increase in adhesion energy (attractive forces) reduces the surface tension, thereby promoting the wetting of the fiber surface by water. As a result, water tends to spread over the fiber surface to achieve the most stable condition (equilibrium state), which in turn leads to an increase in the wetted pore space (hydrophilic pore space) of the DM pore network.

In terms of water management, the increase in temperature reduces the resistance of the DM to the formation of a continuous film or connected conduits of water inside the pores, yielding a redistribution of water and reactant gas within the DM. The decrease in hydrophobicity promotes the accumulation of water into more pores, thereby restricting the reactant gas transport into the catalyst layer, undesirable for efficient fuel cell operation. Upon cooling the fuel cell at shutdown, however, this residual water may be ejected into the flow channels, blocking the available transport paths for reactant gases during start-up. Some studies[19-23] suggest that even though any possible temperature change within the porous media can alter the wettability characteristics of the porous media, the change in operating temperature may result in uneven temperature distribution within the DM. The temperature variation within the pores of the DM can induce a favorable internal pressure gradient, promoting the displacement of the gas phase.

One other distinctive observation that can be drawn from Fig. 2 is that the change in hydrophilic pore distribution with increasing temperature is more pronounced in the macropores (radius range from 1 to 100 μm). Current results reveal that the relatively larger pores (macropores, pore radius >1 μm) are subjected to higher change of wettability characteristics with temperature than that of the minute pores in the MPL (pore radius from 0.01 to 0.1 μm). The smaller effect of temperature on the micropores may be attributed to the rigid and compact structure of the MPL. As explained above, the increase in temperature causes a decrease in interfacial tensions, promoting the wetting of the fiber surface by water. In these experiments, water and octane were used as working fluids to determine the hydrophilic and the total (hydrophilic and hydrophobic) pore network of the DM, respectively. However, during these experiments, the compactness and rigidity of the MPL may have restricted the imbibition of water through the available minute pores of the MPL, therefore impeding observation of the apparent effects of temperature on the pore characteristics of the MPL. As a result, the loss of hydrophobicity is measured to be relatively smaller compared to the ordinary macro-DM substrate due to the restricted access of the water to the available pores of the MPL.

In actual fuel cell operation, the scenario is not much different. The compact nature of the MPL provides an additional resistance, restricting the diffusion of generated water from the catalyst layer through the macroporous substrate. In addition, our previous study,[11] along with that of Gostick et al.,[31] revealed that the MPL is found to contain considerably fewer hydrophilic pores and it is almost exclusively hydrophobic in nature, further hampering the imbibition of liquid into its minute pores. Therefore, even though the temperature has a considerable impact on the surface tension, the higher liquid water resistance of the MPL limits the accessible surface area for water imbibition, suppressing the effect of temperature on the interaction of the water molecules and carbon fiber within the pores of the MPL.

Dual pore network surface area.— The mixed wettability of a porous fuel cell DM is directly linked to the respective proportions of hydrophilic and hydrophobic surface area, which has a large degree of influence on the liquid water transport mechanism in the DM,[19,20] because the nature of the pore surface governs the wetting behavior of the fluids, therefore controlling the transport process within the pores of the DM.

The specific hydrophilic surface area of each DM sample was measured at different temperatures (20, 50, and 80°C) and is shown in Table II. At room temperature, among SGL 24 series, SGL 24BC (5% PTFE) is found to have the higher hydrophilic specific surface area (54.1 m^2/g), demonstrating that rendering the DM with more hydrophobic agent leads to a more hydrophobic surface area. However, as the temperature is further increased to 80°C, the hydrophilic surface area is found to increase for the DM samples. This can be attributed to the possible loss of hydrophobicity with increasing

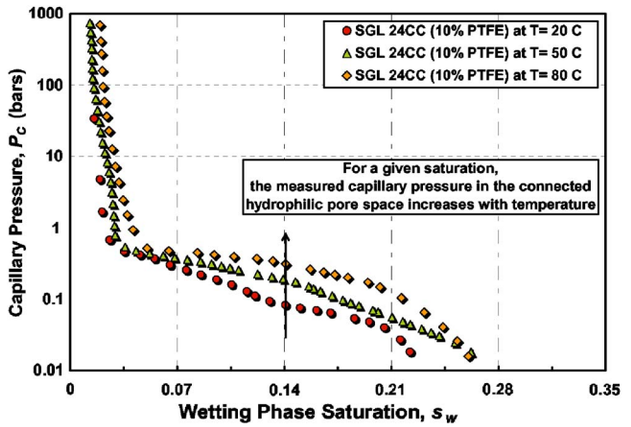

Figure 3. (Color online) Measured capillary pressure vs wetting phase saturation for the connected hydrophilic pore network of SGL 24CC (10% PTFE) carbon paper at 20, 50, and 80°C.

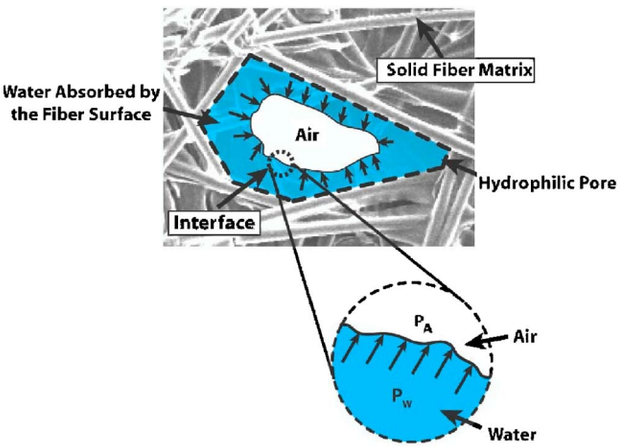

Figure 4. (Color online) Schematic of the behavior of the liquid water (wetting phase) and air (nonwetting phase) in a hydrophilic pore.

temperature. Furthermore, the tabulated results also indicate that the significance of the degree of PTFE loading seems to be diminished with increasing temperature, confirming the results shown in Fig. 2. The measured hydrophilic surface area of SGL 24BC (5% PTFE) and SGL 24DC (20% PTFE) at 80°C is found to be 58 and 55 m^2/g, respectively, yielding a similar hydrophilic surface area regardless of the amount of PTFE loading.

Interconnected hydrophilic pore network and capillary pressure curves.— Water retention characteristics of the DM.— The mass-transport rate through the pores of the DM is closely related to the available connected hydrophilic pore space governing the water retention characteristics of a fuel cell DM. Basically, the water retention capacity (water storage) is a measure of available connected pore space of the fuel cell DM that can store water. From a fuel cell perspective, the stored water or residual water in the DM presents technical challenges, especially in terms of adapting automotive-based fuel cell systems to next-generation vehicles. Many efforts are now focused on minimizing the residual water inside a stack to eliminate the possible degradation during start-up in frozen conditions and to reduce the parasitic purge energy for activating rapid start-up.[32] As such, the water retention characteristic of the DM is a key parameter for proper DM material selection.

To evaluate the degree of change in the capillary transport characteristics of the connected hydrophilic pore network, spontaneous capillary imbibition tests were performed at different temperatures (20, 50, and 80°C). The connected hydrophilic pore volume and the capillary pressure-water saturation of the hydrophilic pore network were measured at specified temperatures for all DM samples. Figure 3 shows the measured capillary pressure vs water saturation of the SGL 24CC (10% PTFE) carbon paper. Increasing the temperature appears to have an impact on the water retention or self-wetting characteristics of the DM. For a given wetting phase saturation, the capillary pressure tends to increase with temperature, as seen in Fig. 3.

The present results reveal that the capillary pressure in a hydrophilic pore increases with temperature, facilitating the transport of nonwetting phase from the connected hydrophilic pore space. The reason for such a change in capillary pressure can be explained through the concept of the immiscible fluid transport at the microscopic pore level. In any pore, the wetting phase is preferentially "adsorbed" (adherence of molecules to the surface of solids) by the solid fiber matrix, while the nonwetting phase is surrounded by the wetting phase. So in a hydrophilic pore, the liquid water, wetting phase, is absorbed by the solid pore matrix, whereas the air, nonwetting phase, is confined and surrounded by the water in the pore enclosure, as illustrated in Fig. 4.

Spontaneous liquid water imbibition is a natural process and requires the existence of interconnected hydrophilic pores. Therefore, only the connected hydrophilic pore space of the tested DM is of interest in the analysis of these imbibition experiments. An increase in temperature facilitates the adsorption of water by the fibers, increasing the volume of imbibed water in the hydrophilic pore due to the increased adhesion energy. The increase in amount of water (wetting phase) causes an increase in the exerted pressure on the nonwetting phase. This, in turn, distorts the imbalance at the interface of the wetting and nonwetting phase, increasing the capillary pressure. Eventually, once the threshold pressure is reached, the nonwetting phase (gas) is displaced from the hydrophilic pore.

Capillary pressure-saturation curves of total pore network.— The microscale parameters measured at room temperature may not be readily applicable to modeling of the actual drainage process of the DM in typical fuel cell environments, where operating temperature is significantly different than the room temperature. To the best of our knowledge, no systematic studies related to the temperature dependence of drainage process for a fuel cell DM have been published.

In order to assess the significance of temperature on the drainage of air-water capillary pressure-saturation curves, highly wetting liquid octane was utilized as a working liquid to obtain the total (hydrophilic and hydrophobic) pore network capillary pressures as a function of nonwetting phase saturation. The experiments were performed at 20 and 50°C. (The higher evaporation rate of octane at 80°C was prohibitive). Using the octane-air capillary pressure-saturation data, the equivalent water-air capillary pressure was calculated by means of the Young–Laplace equation[33] given in Eq. 1

$$P_c = P_{\text{nw}} - P_w = \frac{2\gamma \cos \theta}{r} \qquad [1]$$

Figure 5 depicts the capillary pressure vs the nonwetting phase saturation of the pore network for the DM samples, SGL 24BC, SGL 24CC, and SGL 24DC. For a given nonwetting phase saturation, the capillary pressure decreases as the temperature increases from 20 to 50°C for SGL 24BC and SGL 24CC carbon papers. SGL 24DC carbon paper (coated with 20% PTFE) seems to behave in the same manner up to saturation at 0.4. However, at the high-saturation region ($s_{\text{nw}} > 0.4$), the temperature effect on the capillary pressure curves for SGL 24DC cannot be clearly distinguished, because the capillary pressure measurements at both 20 and 50°C yield similar quantitative values. This observation suggests that for a DM coated with higher PTFE loadings, the effect of temperature on the capillary pressure seems to be more pronounced at low saturations

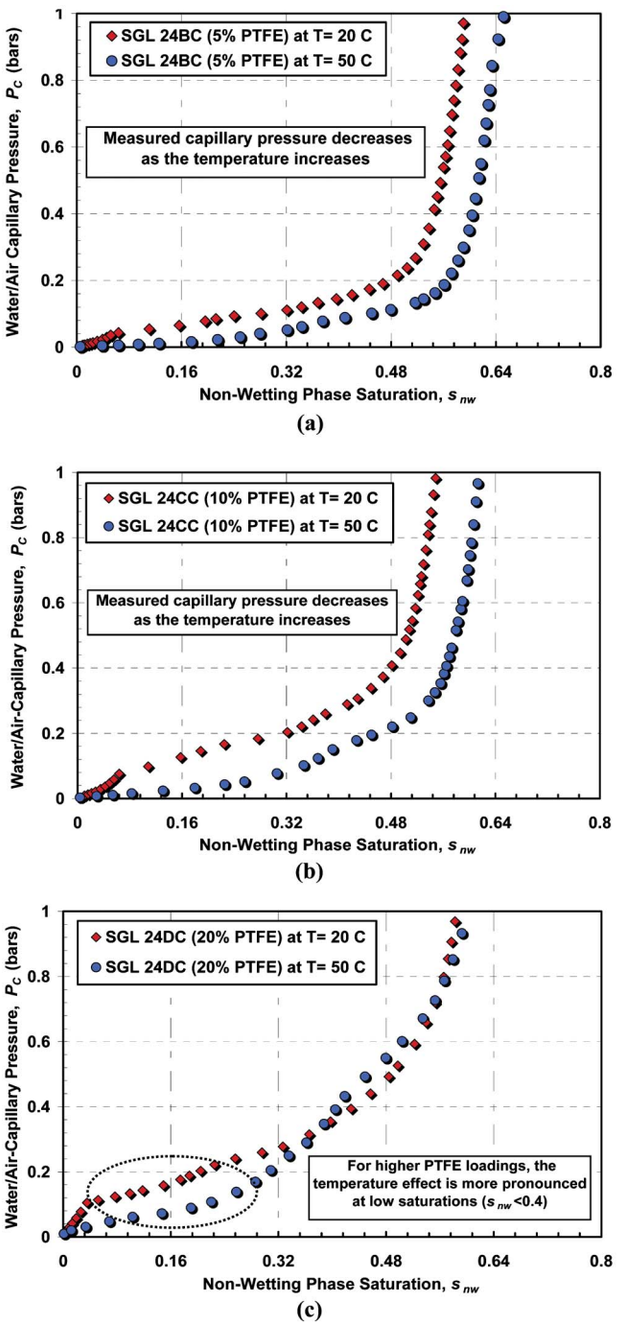

Figure 5. (Color online) Measured capillary pressure vs nonwetting saturation at 20 and 50°C of (a) SGL 24BC, (b) SGL 24CC, and (c) SGL 24DC.

($s_{nw} < 0.4$) and low temperatures (~20°C), potentially because of the higher dominance of wettability characteristics on the capillarity of the pores at this specified condition.

Physically, the temperature sensitivity of the capillary transport in fuel cell DM cannot be explained through the concept of the surface tension alone. The pertinent studies in soil science[19,20] reveal that the interfacial tension and wettability characteristics are strongly coupled. Any increase in temperature influences the molecular interaction between the flowing fluids and solid pore matrix, which is followed by a subsequent increase in adhesion energy. Consequently, the increase in adhesive forces alters the intrinsic contact angle of the (flowing) fluid with the solid surface. (The contact angle is considered as a measure of the surface wettability.[30]) The pertinent studies in soil science approach this issue in different fashions. In some studies[19] the possible changes in the capillary transport with temperature are attributed to the adsorption and desorption of the polar components between the liquid phase and solid pore structure. However, some claim that the corresponding change in viscosity of the flowing fluids, the increase of impurity concentrations, and the alteration of sand compaction with temperature are the potential factors affecting the capillary transport mechanism.[19]

Even though a number of possible hypotheses are available to explain the temperature effect for soil beds, the Young–Laplace capillary theory, as shown in Eq. 1, offers an indispensable means for providing a physical platform for the interpretation of these results in terms of fuel cell DM. In accordance with Eq. 1, the surface tension and contact angle parameters mainly govern the corresponding macroscopic change in capillary pressure in response to altering the temperature, assuming there is no change in pore size due to the temperature difference.

Consider a water droplet (nonwetting phase) sitting on a PTFE-coated carbon fiber and surrounded by air (wetting phase), as shown in Fig. 6. The intermolecular forces acting at the interface of the droplet and pore surface creates a state of tension in the surface of the droplet, known as surface tension.[19,34] The surface tension is prone to be suppressed with increasing temperature due to the enhanced stored energy within the molecules. As the temperature increases, the adhesive (attractive) forces between the water and fiber molecules increase at the interface, promoting the adhesion of the water molecules on the fiber surface. Because of the enhanced adhesion forces with increasing temperature, macroscopically, the water droplet tends to spread over the fiber surface, moving toward a more stable condition inside the pore. As the water droplet (nonwetting phase) covers more surface area (the contact area) with increasing temperature, the apparent contact angle between the fiber surface and droplet decreases, as illustrated in Fig. 6. In a recent study by Oszcipok et al.,[35] the contact angle measurements revealed that the contact angle on the DM is prone to decrease with increasing temperature due to the possible loss of hydrophobicity, in good agreement with this physical explanation. Note that the capillary pressure arises from the imbalance in pressure across the interface between two immiscible fluids. Therefore as the droplet approaches an equi-

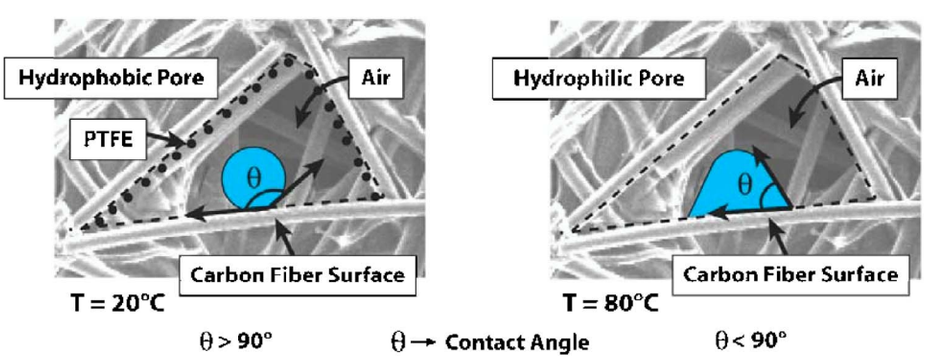

Figure 6. (Color online) Schematic of liquid water droplet behavior inside the pore of a DM at different temperatures.

librium state or mostly stable state (i.e., covering more surface area), the imbalance of molecular forces at the interface diminishes, yielding a lower capillary pressure.

In summary, the surface interaction between the phases and pore surface is greatly influenced by the temperature. Any increase in temperature is accompanied by an increase in the adhesion forces that reduce the surface tension and the intrinsic contact angle at the phase interface. This, in turn, decreases the capillary pressure of the DM as formulated in Eq. 1.

Capillary pressure-saturation correlation for fuel cell DM: A unified approach.— The characteristic capillary pressure-saturation relationship of the fuel cell DM is of utmost importance, especially for fuel cell modelers, to accurately predict the liquid saturation profiles within the operating PEFC. The inherent limitations and the ineffectiveness of the traditional Leverett approach proposed by Leverett[8] and Udell[9] for highly heterogeneous thin-film fuel cell media have been addressed in detail in our previous publications.[1,11,12] One of the main motivations of this publication series is to provide the most appropriate form of the Leverett approach (based on actual experimental data) for accurate prediction of the capillary pressure of tested fuel cell DM as a function of the hydrophobic agent (PTFE) content and the operating conditions, including compression and temperature. To date, in fuel cell modeling studies, the following calibrated form of the standard Leverett approach for hydrophobic fuel cell porous media proposed by Pasaogullari and Wang[36] and Nam and Kaviany[37] has been commonly employed to characterize the liquid water transport within the porous fuel cell DM

$$P_C = \gamma \cos\theta \left(\frac{\varepsilon}{k}\right)^{1/2} J(s)$$

$$J(s) = \begin{cases} 1.417(1-s) - 2.120(1-s)^2 + 1.263(1-s)^3 & \text{if } \theta < 90^\circ \\ 1.417s - 2.120s^2 + 1.263s^3 & \text{if } \theta > 90^\circ \end{cases} \quad [2]$$

The first two parts of this comprehensive study[11,12] were devoted to determining a proper empirical relationship that accurately correlates the capillary pressure as a function of liquid saturation, hydrophobic additive content, and compression pressure of the tested fuel cell DM samples. The final step includes the integration of experimentally observed temperature effects into the previous empirical correlation[12] to deduce a unified form of capillary pressure-saturation saturation, incorporating the relevant material and the operational conditions. Previously, the final form of the empirical capillary pressure-saturation correlation was introduced as[12]

$$P_C = \gamma 2^{0.4C} \sqrt{\frac{\varepsilon_c}{k}} K(s_{nw}) \quad [3]$$

where C, ε_c, k, and γ represent the compression pressure, compressed porosity, absolute permeability, and surface tension, respectively. $K(s_{nw})$ represents the empirical Leverett function,[11] correlating the capillary pressure as a function of liquid saturation and PTFE content of the tested DM samples. The reduction in effective pore size due to the compression of the DM was incorporated by the effective porosity parameter that was determined through the specific strain-stress relations of the tested DM samples described in[12]

$$\varepsilon_c = \left(\frac{0.9}{1 + s_{TR}} + 0.1\right)\varepsilon_o \quad [4]$$

where ε_o and s_{TR} represent the uncompressed porosity and the compressive strain of the DM. The compressive strain (s_{TR}) is a characteristic property of a specified DM and was experimentally determined as[12]

$$s_{TR} = \begin{cases} -0.0083C^2 + 0.0911C & \text{SGL 24 - Series} \\ -0.0046C^2 + 0.0843C & \text{SGL 10BB} \end{cases} \quad [5]$$

Recognizing the fact that the surface tension of water is highly sensitive to temperature, an appropriate approach, therefore, would be to impose the temperature effect into the surface tension term. The surface tension of water as a function of temperature is given by[38]

$$\gamma = -1.78 \times 10^{-4}(T) + 0.1247 \quad [6]$$

where temperature, T, is in Kelvin. The benchmark capillary pressure-saturation measurements of SGL 24 carbon paper series were categorized according to the operating temperature and the PTFE loadings of the DM (ranging from 5 to 20 wt %.). The temperature sensitivity of the tested SGL 24 series carbon paper DM was empirically taken into account by introducing the term $(293/T)^6$, which is defined based on the wide range of experimental data. This additional empirical term allows incorporation of the effects of temperature on the capillary pressure characteristics of the tested DM samples and it can vary or have different functional forms for other commercial DMs which are not treated in this study. In addition, instead of the traditional standard Leverett J-function [$J(s_{nw})$], the empirically derived Leverett function [$K(s_{nw})$] presented in the first phase[11] of this paper series was employed in the unified approach.

After integration of all these representative relationships into the main framework of the traditional approach, the form of Leverett approach appropriate for the tested SGL 24 series DM (coated with MPL) within the range of testing conditions (i.e., $20^\circ C \le T \le 80^\circ C$ and $0 \le C \le 1.4$ MPa) is found as

$$P_C = (293/T)^6 \gamma(T) 2^{0.4C} \sqrt{\frac{\varepsilon_c}{k}} K(s_{nw}) \quad [7]$$

$$K(s_{nw}) = \begin{cases} (\text{wt \%})[0.0469 - 0.00152(\text{wt \%}) - 0.0406s_{nw}^2 + 0.143s_{nw}^3] + 0.0561 \ln s_{nw} & 0 < s_{nw} \le 0.50 \\ (\text{wt \%})[1.534 - 0.0293(\text{wt \%}) - 12.68s_{nw}^2 + 18.824s_{nw}^3] + 3.416 \ln s_{nw} & 0.50 \le s_{nw} \le 0.65 \\ (\text{wt \%})[1.7 - 0.0324(\text{wt \%}) - 14.1s_{nw}^2 + 20.9s_{nw}^3] + 3.79 \ln s_{nw} & 0.65 < s_{nw} < 1.00 \end{cases}$$

where C, ε_c, k, and γ represent the compression pressure, compressed porosity, absolute permeability, and surface tension, respectively. The parameters in $K(s_{nw})$, namely, (wt %) and s_{nw} are PTFE weight percentage and nonwetting liquid saturation, respectively. This unique empirical function [$K(s_{nw})$] is capable of correlating the capillary pressure as a function of liquid saturation and hydrophobic additive loading of the tested DM samples.[11] The PTFE parameter, (wt %), embedded into the modified Leverett function [$K(s_{nw})$] adjusts the degree of hydrophobicity of the tested DM. It also implicitly accounts for variations in internal contact angle, thus eliminating the need for the selection of a single and unrealistic surface contact angle.

Substituting all these subfunctions into the empirical framework, the representative empirical correlation describing the capillary

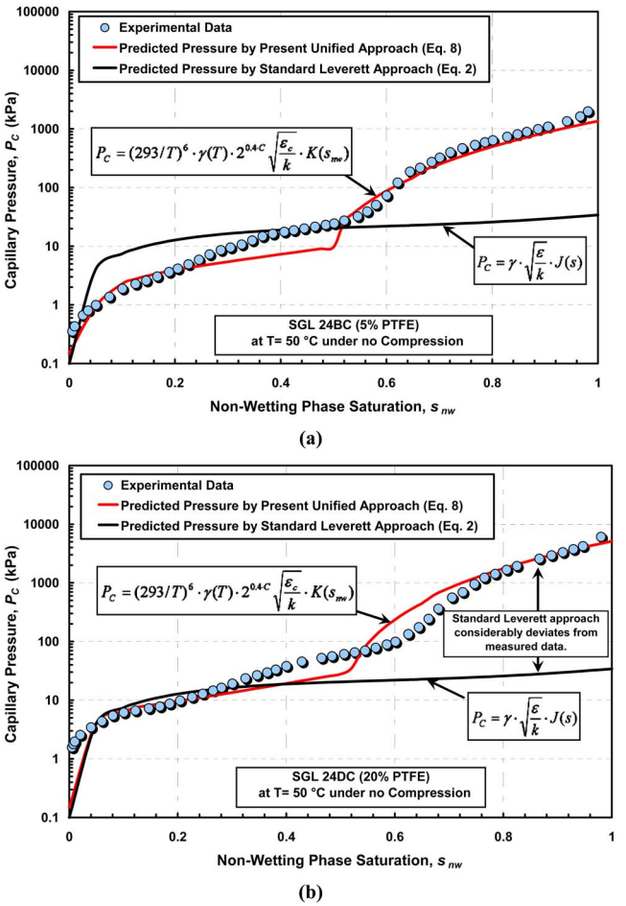

Figure 7. (Color online) Comparison of the present unified approach (Eq. 8), the standard Leverett approach (Eq. 2), and the experimental data for (a) SGL 24BC at 50°C and (b) SGL 24DC at 50°C under no compression.

pressure of the tested SGL 24 series (SGL 24BC, CC, and DC) carbon papers as a function of the relevant transport parameters is found as

$$P_C = (293/T)^6 \gamma(T)\, 2^{0.4C} \times \left[\left(\frac{0.9}{1 + (-0.064C^2 + 0.1661C)} + 0.1 \right) \frac{\varepsilon_o}{k} \right]^{1/2} K(s_{nw}) \quad [8]$$

Similarly, substituting the compression stress-strain relationship (given in Eq. 5) of SGL 10BB DM, the final form of the modified capillary pressure function for SGL 10BB carbon paper becomes

$$P_C = (293/T)^6 \gamma(T)\, 2^{0.4C} \times \left[\left(\frac{0.9}{1 + (-0.0046C^2 + 0.0843C)} + 0.1 \right) \frac{\varepsilon_o}{k} \right]^{1/2} K(s_{nw}) \quad [9]$$

Validation and comparison.— Figure 7 presents the capillary pressure predictions of the present approach (Eq. 8) and the traditional Leverett approach along with the measured capillary pressure for SGL 24BC (5% PTFE) and SGL 24DC (5% PTFE) at 50°C. In these comparisons, the contact angle term (cos θ) originally given in Udell's correlation (Eq. 2) has been assumed to be one in order to perform the comparison with the maximum possible value of the capillary pressure that can be predicted by using the standard Leverett approach given in Eq. 2. As shown in Fig. 7, the standard Leverett approach appears to be incapable of tracking the measured capillary pressure over the entire saturation domain, with the most significant deviation at high saturations, $s_{nw} > 0.5$ (underpredicting more than 100% of the measured values). Even in the low-saturation region ($s_{nw} < 0.5$) the average uncertainty associated with the prediction of the standard Leverett approach is around ±70% of the measured values. While the traditional Leverett approach underpredicts the measured values in this manner, the present empirical approach (Eq. 8) captures the effect of temperature more accurately, predicting the measured capillary pressures (within the uncertainty of ±14% of the measured data) via successfully tracking the complex shape of the measured curves over the entire saturation domain.

The present results also confirm that the Leverett approach in its original form (Eq. 2) cannot appropriately describe the transport characteristics of a fuel cell DM. The significant deviation likely originates from the structural differences between the fuel cell DM and the soil beds. The traditional Leverett approach was derived from the capillary pressure measurements of the various isotropic soil beds with uniform wettability. However, the fuel cell DM exhibits heterogeneous complex internal architecture with mixed wettability. The existence of bimodal pore size distribution in fuel cell DM bifurcates the transport paths, complicating the transport phenomena. Because the present unified empirical approach is deduced from direct experimental measurements of fuel cell DM the connection between the capillary pressure and the relevant transport parameters is precisely linked to the operating conditions through the extensive experimental database. The generalized form of the present approach, as given in Eq. 7, provides the flexibility to predict the capillary pressure by scaling the operating conditions and the governing DM parameters.

To further assess the prediction accuracy of the modified Leverett approach, a comparison with the measured and the predicted capillary pressure (using Eq. 9) of SGL 10BB carbon paper DM at 50°C under 1.4 MPa compression was performed and the results are shown in Fig. 8. The capillary pressure predicted by the standard Leverett approach (Eq. 2) is also presented in Fig. 8. Within the saturation range of 0–0.5 (Fig. 8a), the present empirical fit successfully predicts the measured capillary pressure at the given conditions with an uncertainty of +7% of the measured value, while the standard Leverett approach yields much greater uncertainty of up to +30% of the measured value within this saturation range ($0 < s_{nw} < 0.5$). When the capillary pressure predictions were compared over the entire saturation domain ($0 < s_{nw} < 1$), the present unified approach is much better able to track the complex shape of the measured capillary pressure, whereas the gap between the measured values and the prediction of the standard Leverett approach vastly increases, especially at high saturations ($s_{nw} > 0.5$). These results also support the fact that besides the mixed wettability characteristics of the DM, the standard Leverett approach in its original form is also insufficient to incorporate the coupled effect of temperature and compression, thereby failing to capture the corresponding changes in the capillary pressure of SGL 10BB (5% PTFE) carbon paper.

In order to validate the effects of temperature with the experimental observations, the capillary pressure of a DM coated with 5% PTFE over a wide range of temperatures was predicted by the present approach given for SGL 24 series (Eq. 8). Figure 9 depicts the predicted capillary pressures vs the nonwetting saturation at different temperatures (20, 40, 60, and 80°C). For a given saturation, the capillary pressure exhibits a decrease in response to the increase in temperature due to the reduced surface tension. This trend is in good agreement with the previously discussed observations in Fig. 5, thereby supporting the effectiveness of the present approach.

Features and limitations.— The final form of the capillary pressure equation given in Eq. 7 is comprised of three main terms, as shown in Eq. 10. The first term $(293/T)^6 \gamma(T)$ accounts for the effect of temperature. As described, any change in temperature influences the molecular interactions at the solid-liquid interface, therefore affecting the surface tension and wettability characteristics of the fuel cell DM. The corresponding change in surface tension is included in

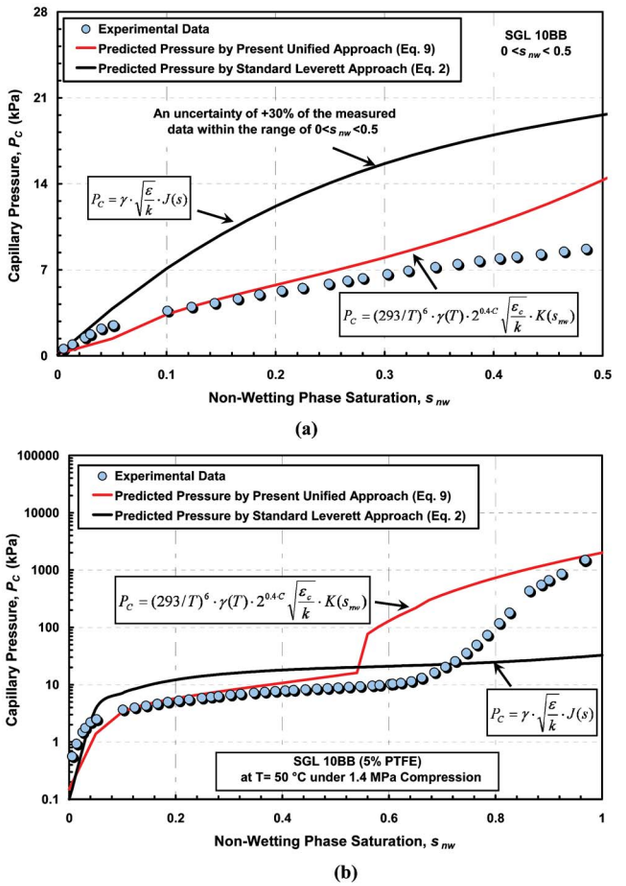

Figure 8. (Color online) Comparison of the present unified approach (Eq. 9), the standard Leverett approach (Eq. 2), and the experimental data for SGL 10BB at 50°C under 1.4 MPa over a saturation range of (a) $0 < s_{nw} < 0.5$ and (b) $0 < s_{nw} < 0.1$.

the analytical framework through both the surface tension term and the empirical parameter, $(293/T)^6$, deduced from broad set of the benchmark data for the tested DM samples. The second term, $2^{0.4\times C}(\varepsilon_c/k)^{0.5}$, embodies the effect of compression on the morphological characteristics of the fuel cell DM. Any compression exerted on the DM causes substantial deformation of the fibers, leading to a reduction in the effective porosity.[12] The corresponding change in effective porosity (given in Eq. 4) is taken into account by an empirical correlation relating the compressive strain and compression pressure. It is worthwhile to emphasize that the compressive strain-stress relation is a characteristic property for each DM and depends on the fabrication process and fiber types and therefore needs to be experimentally determined for each DM type

$$Pc = \underbrace{(293/T)^6\gamma(T)}_{\text{Temperature effect}}\underbrace{2^{0.4C}\sqrt{\frac{\varepsilon_c}{k}}}_{\text{Compression effect}}\underbrace{K(S_{\text{nw}})}_{\text{Mixed wettability}} \quad [10]$$

The final term includes the empirical Leverett function $K(s_{\text{nw}})$[11] applicable for the tested DM samples, which was derived from a wide range of capillary pressure measurements of the tested DM samples with PTFE content ranging from 5 to 20 wt %. This function basically serves to account for the mixed wettability characteristics of the DM, which is not properly treated in original Leverett *J*-function. The connection between the liquid saturation and the mixed wettability characteristics of the DM is linked to the capillary pressure by compilation of the extensive capillary pressure-saturation measurements. Adjusting the PTFE variable (wt %) in the modified function, $K(s_{\text{nw}})$, enables successful determination of the capillary pressure as a function of hydrophobic additive loading of the DM. The variations in internal contact angle, a consequence of the mixed wettability characteristics of the DM, are implicitly embedded into the modified Leverett function, which in turn eliminates the selection of a representative contact angle as an input. Overall, the inclusion of all these unique features into the present empirical approach enables more accurate modeling of capillary pressure over a wide range of PTFE loadings at different fuel cell operational environments.

In terms of limitations, it is important to emphasize that the final functional form of the empirical equation given in Eq. 7 is deduced from the capillary pressure-saturation measurements of SGL 24 series carbon paper including SGL 24BC (5 wt % PTFE), SGL 24CC (10 wt % PTFE) and SGL 24DC (20 wt % PTFE). The experiments were performed at three different temperatures (20, 50, and 80°C) under three compression loadings (0, 0.6, and 1.4 MPa). Therefore the presented unified approach is applicable to the tested DM samples within the temperature range from 20 to 80°C for the compression range from 0–4 MPa. Among the tested DM samples, the unified form of the capillary pressure equation given in Eq. 7 can be modified to any of the tested DM samples by simply substituting the characteristics compressive strain (s_{TR})-compression pressure relation at a given temperature under any compression (within the specified ranges).

In addition, further comparisons with the other available benchmark data for different types of DM (i.e., SGL 10BB carbon paper and E-TEK Elat 1200W carbon cloth) have been performed to cross-check the accuracy of the presented approach. The results presented in this paper series[11,12] show that the present approach yields more accurate predictions, even for these different DM samples, compared to the ones obtained with using the standard Leverett approach. For developing a more generalized approach, additional benchmarking of different DM samples needs to be performed in order to expand the database.

One final note, as also mentioned in other parts of this paper series, is that the present empirical correlation given in Eq. 7 is derived based on the generated data for the DM samples coated with a MPL. Therefore, the porous media of interest herein is a composite structure. The capillary pressure-saturation characteristics of the DM macrosubstrate (without MPL) can be obtained through the specific pore network characteristics of the MPL itself and DM macrosubstrate by using the corresponding the pore size distribution and porosities of these layers. In other words, the characteristic capillary pressure-saturation relationship of the macro-DM substrate (i.e., w/o MPL) can be determined from the given composite relationship in

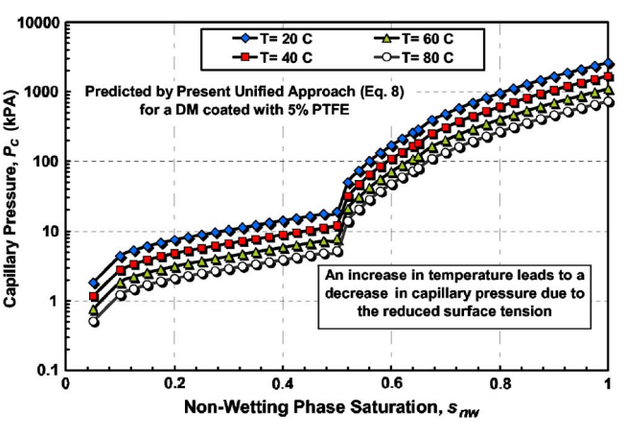

Figure 9. (Color online) Predicted capillary pressure (by the present unified approach given in Eq. 8) vs nonwetting saturation for a DM with 5% PTFE at different temperatures.

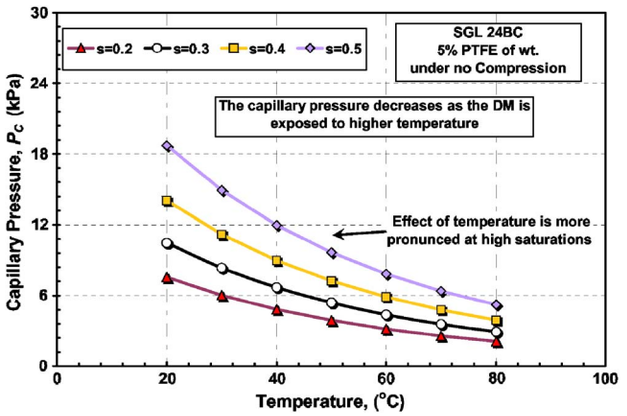

Figure 10. (Color online) Predicted capillary pressure (by the present unified approach given in Eq. 8) vs temperature of SGL 24BC coated with 5% PTFE at constant saturations.

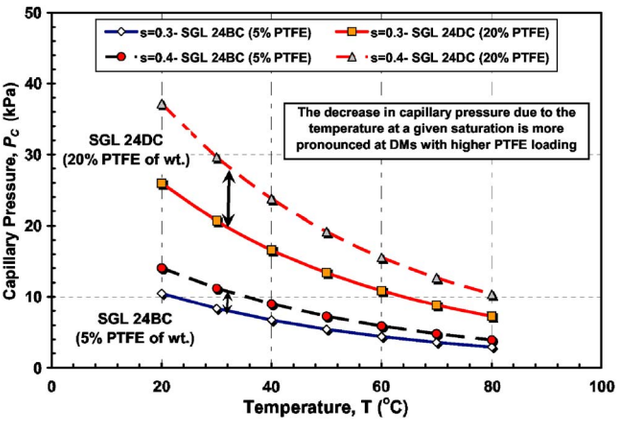

Figure 11. (Color online) Predicted capillary pressure (by the present unified approach given in Eq. 8) vs temperature of SGL 24 BC (5% PTFE) and SGL 24DC (5% PTFE) at constant saturations.

Eq. 7 by extending the capillary pressure-saturation trend of the composite DM from low saturation to high saturations, i.e., eliminating the MPL region. [For example, to predict the behavior in the macro-DM alone for the SGL 24 series, the empirical Leverett-type function, $K(s_{nw})$, given for the saturation range $0 < s_{nw} < 0.5$, can be extended to $0 < s_{nw} < 1$]. In this way, the empirical function for the macro-DM region alone (without MPL) can be estimated before specific experimental data for these materials become available.

Overall, the Leverett approach presented here provides a reliable tool for the description of the capillary pressure in terms of accessible parameters, therefore representing an improvement in the precision of PEFC DM multiphase transport predictions.

Further discussion: Temperature and PTFE sensitivity.— To further elucidate the significance of temperature on the retention characteristics of fuel cell DM, the changes in capillary pressure at given saturation values were probed. Figure 10 depicts the calculated capillary pressure predicted by Eq. 8 of a DM tailored with 5% PTFE vs operating temperature at different saturation values (0.2, 0.3, 0.4, and 0.5), recalling that a PEFC typically operates in a saturation range of 0–0.5.[32] At a given saturation, the capillary pressure is found to decrease with temperature, as expected. However, one distinctive observation drawn from this analysis is that the decrease in capillary pressure with temperature is more pronounced at high saturation ($s_{nw} = 0.5$), whereas at low saturation ($s_{nw} = 0.1$), the temperature seems to have a relatively low impact on the capillary pressure. Physically, in a given pore, the capillary pressure is directly linked to the molecular imbalance at the interface of nonwetting and wetting phase. At high saturation, the imbalance between the interfacial forces is prone to be more suppressed with increasing temperature, yielding a larger decrease in capillary pressure.

Finally, the governing parameters, namely, operating temperature and PTFE content of the DM, were investigated jointly to assess the relative significance of these parameters on the capillary transport. The capillary pressure of SGL 24BC (5% PTFE) and SGL 24DC (20% PTFE) was predicted by means of the present empirical fit (Eq. 8) for constant saturation values at different temperatures. Figure 11 shows the variation in predicted capillary pressure values of the DM as a function of temperature. SGL 24 DC carbon paper appears to exhibit a larger decrease in capillary pressure (from 38 to 10 kPa at $s = 0.4$) as the temperature is increased from 20 to 80°C. For SGL 24BC (5% PTFE), the capillary pressure seems to be relatively less affected by the temperature. Capillary pressure is found to be increased from 2 kPa to 14 kPa as the temperature is increased from 20 to 80°C at $s = 0.4$. In other words, the effect of temperature on the capillary pressure within the pores of the DM appears to be amplified with rendering the DM more hydrophobic. This can be attributed to the fact that the reduction of surface tension with increasing temperature seems to be more severe in the pores of DM tailored with high PTFE loading.

Conclusion

The final part of this paper series is aimed at explicitly investigating the effects of temperature on the multiphase transport characteristics of the fuel cell DM. The benchmark data were generated from a wide set of capillary pressure-saturation measurements performed for various types of fuel cell DM at different temperatures, namely, 20, 50, and 80°C. Temperature is found to be an important factor affecting the transport characteristics of the fuel cell DM. The capillary pressure is observed to decrease with increasing temperature due to the reduced surface tension. Any increase in temperature is also accompanied by the loss of hydrophobicity of the DM, indicating the possible formation of liquid film or connected conduits within the pores of the DM.

Experimentally observed temperature effects were integrated into the empirical correlation derived from the first phase of this study[11,12] to deduce a unified description of capillary pressure-saturation correlation appropriate for the tested fuel cell DM samples as a function of the relevant material properties and the operational environments. The results show that the final form of the present unified approach (given in Eq. 7) well-predicts the capillary pressure as a function of liquid saturation, hydrophobicity, compression of the DM, and operating temperature (within the uncertainty of ±14% of the measured data). Note that the unified empirical approach presented herein is applicable to the tested DM samples within the range of testing conditions (i.e., temperature range from 20 to 80°C and the compression range from 0 to 1.4 MPa).

The key features of the present approach are (*i*) it embodies the nonuniform wettability characteristics of the fuel cell DM, thereby accounting for the variations in transport parameters with full spatial anisotropy of the DM; (*ii*) it accounts for the variations in internal contact angle caused by the nonuniform wettability characteristics, therefore eliminating the need for selection of a single surface contact angle; and finally, (*iii*) it incorporates the effects of compression and temperature on the capillary transport characteristics of the tested DM samples and performs the necessary adjustments to predict capillary pressure as a function of hydrophobic additive content, compression pressure, uncompressed porosity, and temperature.

The characteristic benchmark capillary pressure-saturation correlation presented in this study will help to close the loop between fuel cell modeling studies and missing transport relationships for thin-film porous media and therefore represents an improved step toward achieving an accurate two-phase transport model in fuel cell mod-

eling studies. Our team is currently working on expanding the existing benchmark database to deduce a more generalized correlation for fuel cell DMs. In addition, the development of an advanced fuel cell model using the present benchmark correlations is ongoing work in our laboratory and will be reported in subsequent publications soon.

Acknowledgments

This research is supported by National Science Foundation grant no. CTS-0414319. The authors thank Dr. Alex Sakars from Porotech, Ltd., for performing the MSP experiments and Elise Corbin for her help during the preparation of Fig. 4 and 6.

The Pennsylvania State University assisted in meeting the publication costs of this article.

List of Symbols

C	compression pressure, MPa
P_C	capillary pressure, Pa
P_e	pore entry pressure, Pa
S_{TR}	compressive strain, unitless
T	temperature, °C
k	permeability, m^{-2}
s	saturation, unitless
wt %	weight percentage of hydrophobic additive, unitless

Greek

ε	porosity, unitless
θ	contact angle, degree
γ	surface tension of water-air, N m^{-1}

Subscripts

c	compressed
C	capillary
e	pore entry
g	gas
l	liquid
o	uncompressed
w	wetting phase
nw	nonwetting phase

References

1. E. C. Kumbur, K. V. Sharp, and M. M. Mench, *J. Power Sources*, **168**, 156 (2007).
2. V. Gurau, M. J. Bluemle, E. S. De Castro, Y.-M. Tsou, J. A. Mann, and T. A. Zawodzinski, Jr., *J. Power Sources*, **160**, 1156 (2006).
3. U. Pasaogullari, Ph.D. Thesis, The Pennsylvania State University, University Park, PA (2005).
4. X. Liu, H. Guo, and C. Ma, *J. Power Sources*, **156**, 267 (2006).
5. S. Litster and N. Djilali, in *Transport Phenomena in Fuel Cells*, B. Suden and M. Faghri, Editors, 1st ed., Chap. 5, WIT Press, Southampton, U.K. (2006).
6. S. M. Senn and D. Poulikakos, *J. Heat Transfer*, **127**, 1244 (2005).
7. N. Djilali, *Energy*, **32**, 269 (2007).
8. M. C. Leverett, *Trans. Am. Inst. Min., Metall. Pet. Eng.*, **142**, 152 (1941).
9. K. S. Udell, *Int. J. Heat Mass Transfer*, **28**, 485 (1985).
10. I. Nitta, T. Hottinen, O. Himanen, and M. Mikkola, *J. Power Sources*, **171**, 26 (2007).
11. E. C. Kumbur, K. V. Sharp, and M. M. Mench, *J. Electrochem. Soc.*, **154**, B1295 (2007).
12. E. C. Kumbur, K. V. Sharp, and M. M. Mench, *J. Electrochem. Soc.*, **154**, B1305 (2007).
13. M. Khandelwal and M. M. Mench, *J. Power Sources*, **161**, 1106 (2006).
14. S. He, M. M. Mench, and S. Tadigadapa, *Sens. Actuators, A*, **125**, 170 (2006).
15. L. Dumercy, R. Glises, H. Louahlia-Gualous, and J. M. Kauffmann, *J. Power Sources*, **156**, 78 (2006).
16. C. Bao, M. Ouyang, and B. Yi, *Int. J. Heat Mass Transfer*, **31**, 1040 (2006).
17. H. Y. She and B. E. Sleep, *Water Resour. Res.*, **34**, 2587 (1998).
18. B. H. Samaroo and E. T. Guerrero, *SPEJ*, Paper SPE, 10153 (1981).
19. J. Bachmann and R. R. Van Der Ploeg, *J. Plant Nutrition Soil Science*, **165**, 468 (2002).
20. A. Dominguez, H. Perez-Aguilar, F. Rojas, and I. Kornhauser, *Colloids Surf., A*, **187**, 415 (2001).
21. H. P. Lien and F. H. Wittmann, *Nucl. Eng. Des.*, **179**, 179 (1998).
22. S. A. Grant and A. Salehzadeh, *Water Resour. Res.*, **32**, 261 (1996).
23. A. G. Yiotis, A. G. Boudouvis, A. K. Stubos, I. N. Tsimpanogiannis, and Y. C. Yortsos, *Am. Inst. Chem. Eng. Symp. Ser.*, **50**, 2721 (2004).
24. H. Z. Syed and R. Hackam, in *Proceedings of the 1998* 67th *IEEE Annual Conference on Electrical Insulation and Dielectric Phenomena*, IEEE, p. 100 (1998).
25. A. A. Sinnokrot, H. J. Ramey, and S. S. Marsden, *SPEJ*, **11**(1), 13 (1971).
26. S. K. Sanyal, S. S. Marsden, and H. J. Ramey, *SPEJ*, Paper SPE, 4898 (1974).
27. A. W. Fan, W. Liu, and G. L. Xu, *Heat Transfer Asian Res.*, **35**, 539 (2006).
28. J. Bachmann, R. Horton, S. A. Grant, and R. R. Van Der Ploeg, *Soil Sci. Soc. Am. J.*, **66**, 44 (2002).
29. Y. M. Volfkovich, V. S. Bagotzky, V. E. Sosenkin, and I. A. Blinov, *Colloids Surf., A*, **187-188**, 349 (2001).
30. E. C. Kumbur, K. V. Sharp, and M. M. Mench, *J. Power Sources*, **161**, 333 (2006).
31. J. T. Gostick, M. W. Fowler, M. A. Ioannidis, M. D. Pritzker, Y. M. Volfkovich, and A. Sakars, *J. Power Sources*, **156**, 375 (2006).
32. A. Turhan, K. Heller, J. S. Brenizer, and M. M. Mench, *J. Power Sources*, **160**, 1195 (2006).
33. T. A. Corey, *Mechanics of Immiscible Fluids in Porous Media*, 1st ed., Water Resource Publications, Highlands Ranch, CO (1994).
34. C. T. Miller, G. Christakos, P. T. Imhoff, J. F. McBride, J. A. Pedit, and J. A. Trangenstein, *Adv. Water Resour.*, **21**, 77 (1998).
35. M. Oszcipok, D. Riemann, U. Kronenwett, M. Kreideweis, and M. Zedda, *J. Power Sources*, **145**, 407 (2005).
36. U. Pasaogullari and C. Y. Wang, *J. Electrochem. Soc.*, **151**, A399 (2004).
37. J. H. Nam and M. Kaviany, *Int. J. Heat Mass Transfer*, **46**, 4595 (2003).
38. M. M. Mench, *Fuel Cell Engines*, Chap. 5, John Wiley & Sons, New York (2007).